scientific reports

Check for updates

OPEN

Compensatory lymphangiogenesis is required for edema resolution in zebrafish

Olamide Olayinka, Hannah Ryu, Xiaowei Wang, Asrar B. Malik & Hyun Min Jung✉

Edema, characterized by the accumulation of interstitial fluid, poses significant challenges in various pathological conditions. Lymphangiogenesis is critical in edema clearance, and delayed or inadequate lymphatic responses significantly hinder healing processes. However, real-time observation of dynamic changes in lymphangiogenesis during tissue repair in animal models has been challenging, leaving the mechanisms behind compensatory lymphatic activation for edema clearance largely unexplored. To address this gap, we subjected zebrafish larvae to osmotic stress using hypertonic (375 mOsm/L) and isotonic (37.5 mOsm/L) solutions to induce osmotic imbalance and subsequent edema formation. Intravital imaging of vascular transgenic larvae revealed significant lymphatic vessel remodeling during tissue edema. The observed increase in lymphatic endothelial progenitor cells, alongside the sustained expansion and remodeling of primary lymphatics, indicates active lymphangiogenesis during the recovery phase. We developed a novel method employing translating ribosome affinity purification to analyze the translatome of lymphatic and venous endothelial cells in vivo, which uncovered the upregulation of key pro-lymphangiogenic genes, particularly *vegfr2* and *vegfr3*, during tissue recovery. Inhibition of compensatory lymphangiogenesis impaired edema fluid clearance and tissue recovery. Our findings establish a new model for in vivo live imaging of compensatory lymphangiogenesis and provide a novel approach in investigating lymphatic activation during edema resolution.

Keywords Lymphangiogenesis, Lymphatic vessel, Edema, Zebrafish, VEGFR

Interstitial fluid plays a crucial role in supplying water and nutrients to cells and removing metabolic waste products that do not easily diffuse into the bloodstream[1]. Edema occurs when excessive interstitial fluid accumulates, leading to swelling and increased tissue volume[2]. It is often associated with conditions such as congestive heart failure, kidney disease, liver cirrhosis, and localized injuries[3,4]. The resulting fluid imbalance has significant clinical implications, contributing to pain, impaired mobility, reduced quality of life, and in severe cases life-threatening health conditions[3,4].

Edema clearance is primarily mediated by the lymphatic system, which play a crucial role in fluid balance and immune responses[5,6]. Lymphatic dysfunction can severely impair tissue healing and exacerbate pathological conditions such as cancer metastasis, lymphedema, and organ transplant rejection, where inadequate fluid clearance further promotes disease progression[7–10]. Despite its critical role, the function of lymphangiogenesis in tissue repair has received less attention than angiogenesis in recent decades. Lymphatic dysfunction, particularly in the context of edema, can prevent fluid clearance, leading to persistent swelling, chronic edema, and eventual systemic failure[1,11]. The regrowth and expansion of lymphatic vessels, driven by signaling pathways such as Vegf, and subsequent fluid clearance are essential for efficient tissue recovery[12–15]. However, the precise mechanisms of compensatory lymphangiogenesis during edema resolution remain poorly understood.

The zebrafish (*Danio rerio)* offers powerful and genetically tractable model for studying tissue repair and vascular biology[16,17]. The optical clarity of zebrafish larvae allows for high-resolution imaging of lymphatic vessels, and a range of transgenic tools enable detailed visualization of lymphatic vessel dynamics[18–27]. Given the structural and functional similarities between zebrafish and mammalian lymphatic systems, findings from zebrafish research can provide valuable insights into lymphangiogenesis in higher vertebrates[18–20,22,25–27]. While compensatory lymphangiogenesis has been studied in mammals, much remains unknown about the precise mechanisms that regulate lymphatic vessel remodeling, particularly during fluid accumulation and edema resolution. Investigating this process in zebrafish offers a unique opportunity to explore the kinetics and regulatory networks involved in lymphatic expansion. Additionally, zebrafish and other freshwater teleosts have evolved mechanisms to regulate ion transport and maintain the hyperosmolarity of their interstitial fluid relative

Department of Pharmacology and Regenerative Medicine, University of Illinois College of Medicine, Chicago, IL 60612, USA. ✉email: hmjung@uic.edu

to their external environment[28]. Environmental stressors, such as abrupt changes in salinity, can disrupt this finely regulated osmoregulation, leading to tissue damage and fluid accumulation in extracellular spaces[29–31]. These characteristics make zebrafish an ideal model for investigating the interplay between fluid homeostasis and lymphatics during tissue repair.

In this study, we investigate the dynamic changes in lymphangiogenesis during edemagenic and recovery phases of tissue recovery. Using live imaging in zebrafish, we provide an integrated view of the compensatory lymphatic expansion mechanism that facilitate edema fluid clearance. Our findings offer valuable insights into the molecular and cellular processes driving lymphatic vessel remodeling during edema resolution.

Results

Induction and imaging of osmotic stress-induced edema in zebrafish

Freshwater teleosts like zebrafish have adaptive mechanisms to regulate interstitial fluid balance in response to changes in water osmolarity[28]. Osmoregulatory dysfunction, especially under hypertonic conditions, leads to tissue damage and fluid accumulation in extracellular space, a hallmark of edema[29–31]. To investigate the mechanisms of edema formation and fluid clearance, we developed an optimized method for inducing edema in zebrafish larvae (Fig. 1A). Embryos were initially maintained in isotonic egg water until 2 days post-fertilization (dpf). At this stage, the embryos were dechorionated and exposed to hypertonic stress (3x Danieau buffer, 375 mOsm/L) for 24 h. Following this, larvae were returned to isotonic egg water (0.3x Danieau buffer, 37.5 mOsm/L), inducing rapid osmotic imbalance. Edema development was tracked using brightfield time-lapse imaging during the 3–4 dpf period (Supplementary Video 1).

We performed eleven independent experiments, each with 20 larvae, and achieved over a 90% success rate in edema induction (Fig. 1B). By 4 dpf, edema was visibly prominent, affecting the entire body compared to untreated controls (Fig. 1C and Supplementary Fig. 1A). Initially, the pericardial area was the first site of swelling, followed by the yolk and trunk regions (Fig. 1D). Quantitative analysis of anatomical areas from a lateral view showed a significant increase in edema, including a 3.32-fold expansion in the pericardial area (Fig. 1D), a 1.60-fold increase in the yolk area (Fig. 1E), and a 1.13-fold increase in the trunk area (Fig. 1F). No significant change was observed in the head region at this time point (Fig. 1G). All measurements were normalized to fish length to account for potential developmental variation and size difference that may arise due to osmotic stress[32]. A dorsal view revealed pronounced swelling around the yolk, which was less evident from the lateral views (Fig. 1H).

To determine the time course of edema formation, larvae were exposed to hypertonic conditions for 18, 24, or 48 h before returning to isotonic conditions. The number of edematous larvae increased with prolonged exposure to hypertonic stress (Supplementary Fig. 1B). A control experiment confirmed that edema was only induced when larvae transitioned from hypertonic to isotonic conditions (Supplementary Fig. 1C, D). Additionally, edema could be induced even when the hypertonic exposure was delayed by one day (hypertonic exposure at 3–4 dpf followed by osmotic stress at 4–5 dpf), demonstrating the flexibility of this protocol across different developmental stages (Supplementary Fig. 1E). These results confirm the reproducibility of edema induction and its effective monitoring in real-time in zebrafish larvae.

Edema resolution in zebrafish larvae

To investigate edema resolution, we tracked fluid clearance over time following edema induction. After 24 h of hypertonic stress and 24 h in isotonic conditions, larvae were raised in isotonic egg water until 8 dpf (Fig. 1A). Across eleven independent experiments (Fig. 1B), we found that about 55–70% of larvae spontaneously resolved their edema, while others exhibited persistent swelling (Fig. 1I). Larvae with persistent edema showed extensive fluid accumulation throughout the body, including the head, which was unaffected at earlier stages (Fig. 1I). In contrast, edema-free larvae returned to a morphology indistinguishable from untreated controls (Fig. 1I,J).

Daily measurements of edema progression in individual larvae revealed that the first 24-hour period (4–5 dpf) of edema formation was critical for determining whether larvae would recover or remain edematous (Fig. 1K). These findings demonstrate the power of this model in visualizing both the formation and resolution of edema in zebrafish larvae.

Lymphatic vessel remodeling during edema resolution

Lymphatic vessels are crucial for fluid recovery during edema by absorbing interstitial fluid from swollen areas[5,6]. To investigate how lymphatics respond during edema progression, we examined lymphatic vasculature in *Tg*(*mrc1a:egfp; kdrl:mcherry*) larvae at 9 dpf. In comparison control larvae raised in osmotically balanced condition (Fig. 2A–C), "edema-free" recovered larvae exhibited significant lymphatic remodeling, with enhanced formation of thoracic duct (TD), intersegmental lymphatic vessels (ISLVs), dorsal longitudinal lymphatic vessels (DLLVs), and lateral lymphatics (LL) (Fig. 2D–F). Notably, the TD showed a 1.5-fold increase in size in the edema-free larvae compared to controls (Fig. 2C,F,G). Furthermore, there was an increased number of lymphatic endothelial cell (LEC) nuclei in the DLLVs (Fig. 2H). Quantitation of LEC nuclei was analyzed using *Tg*(*fli1a:nEGFP; lyve1b:dsRed*). Additionally, the LLs showed accelerated development, with more LL segments present in edema-free larvae than in controls (Fig. 2I). No significant changes were observed in the ISLVs (Fig. 2J).

Craniofacial lymphatics, which arise from lymphangioblasts in the common cardinal vein and primary head sinus at 1.5 dpf[22,33], also showed enhanced development in recovered larvae at 9 dpf. The control larvae maintained in regular egg water displayed stereotypic facial lymphatic development (Fig. 2K–M). The edema-free larvae exhibited extended facial lymphatics with a marked increase in craniofacial lymphatic surface area (Fig. 2N–P). Notably, there was a significant enlargement of the surface area of the facial lymphatics (Fig. 2Q) and increase in LEC numbers within the lateral facial lymphatics (LFL), medial facial lymphatics (MFL), otolithic lymphatic vessel (OLV), and lymphatic branchial arches (LAA) (Fig. 2R). Unusual lymphatic sprouts emerging

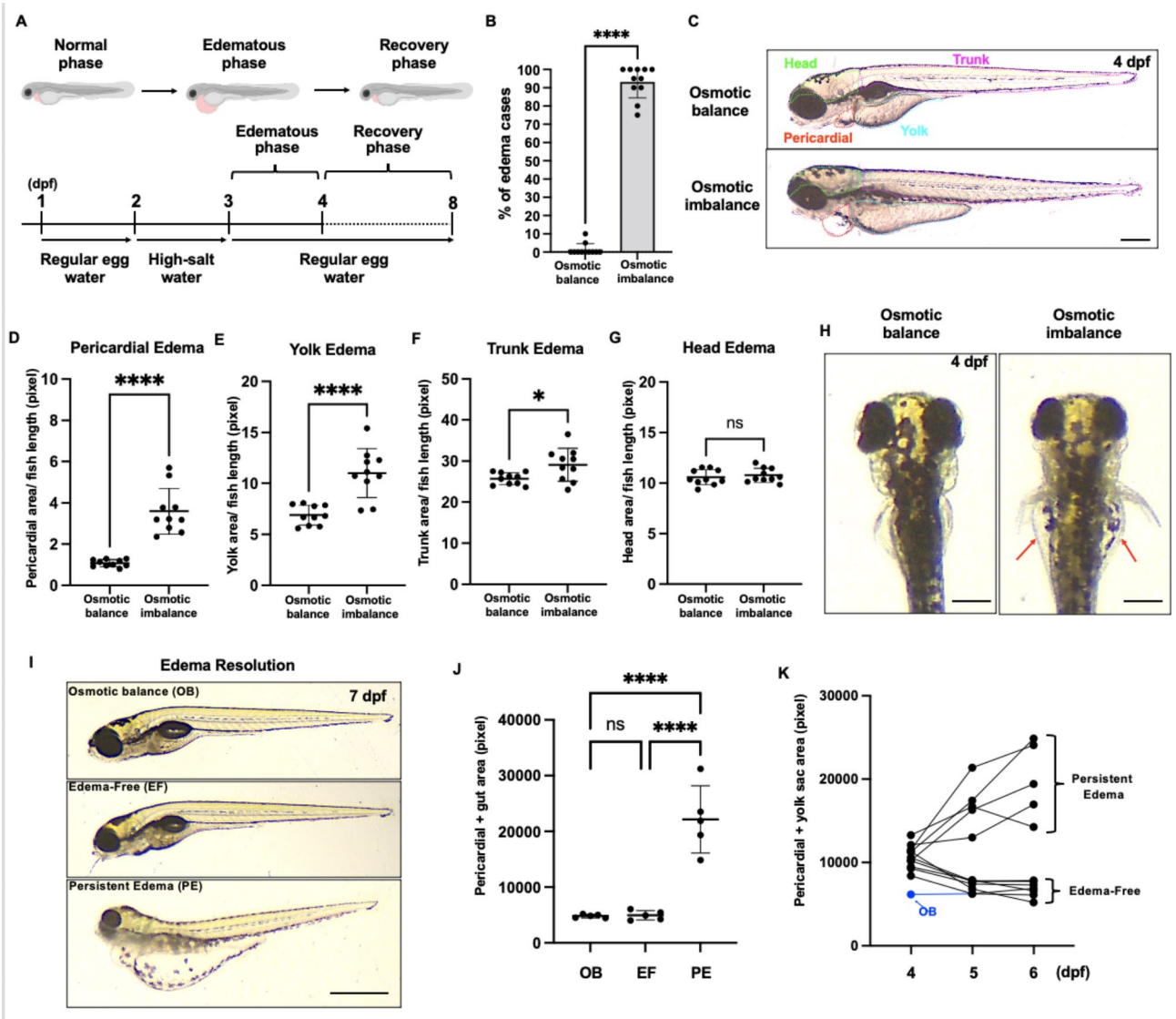

Fig. 1. Zebrafish model of edema formation. (**A**) Schematic showing the experimental workflow from osmotic stress induction to edema formation and resolution. (**B**) Percentage of edematous larvae in osmotically balanced and osmotically imbalanced conditions at 4 dpf. Individual data points represent an independent experiment, and 20 larvae were used for each experiment. (**C**) Representative brightfield images showing lateral views of osmotically balanced (top) and osmotically imbalanced (bottom) 4 dpf zebrafish larvae. The dotted outline illustrates the boundary for edema area quantification in different parts of the body. *Casper* fish were used for imaging. (**D**–**G**) Quantification of pericardial area (**D**), yolk area (**E**), trunk area (**F**), and (**G**) head area. (**H**) Representative brightfield images showing the dorsal view of osmotically balanced (left) and osmotically imbalanced (right) zebrafish larvae. Red arrows indicate edema in the lateral side of the yolk area. (**I**) Representative images of osmotic balance (OB), edema-free (EF), and persistent-edema (PE) larva at 8 dpf. *Casper* fish were used for imaging. (**J**) Quantitative analysis of the pericardium and gut areas. Each dot represents an individual larva. (**K**) Line graph showing edema progression from 4–6 dpf. Each line represents the progressive change in the pericardial + yolk sac surface area of individual larvae over the experiment time course. The blue line is the larva raised in an osmotically balanced solution as a control. Scale bar = 500 µm (**C**,**H**,**I**). ns, not significant; $^{*}p < 0.05$; $^{****}p < 0.0001$.

from the common cardinal vein toward the previously swollen pericardial region were observed infrequently in a small portion of larvae (3 of 15 edema-free larvae), although their functional role in edema recovery remains unclear (Fig. 2P and Supplementary Video 2). Overall, these findings indicate that edema resolution triggers a broad activation of the lymphangiogenic program.

Induction of lymphangiogenesis in response to edema

We next investigated how edema influences the development of lymphatic vasculature. To visualize lymphangiogenesis at the onset of osmotic stress-induced edema, we imaged and quantitated the highly

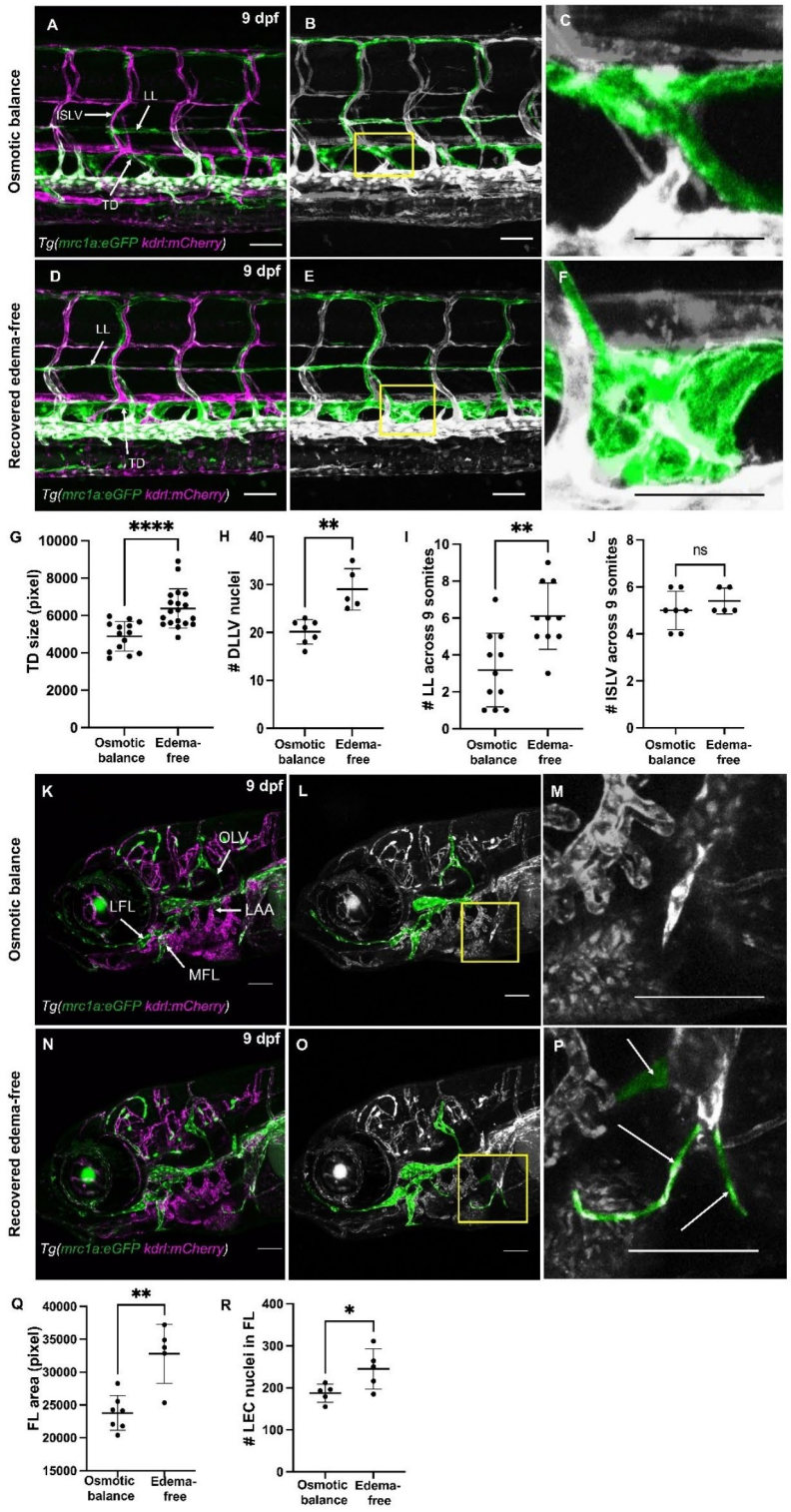

stereotypic lymphatic vasculature in the trunk of zebrafish larvae (Fig. 3A). The parachordal lymphangioblasts (PLs) represent a transient population of lymphatic progenitors that localize to the horizontal myoseptum at 2–3 dpf (Fig. 3B). These lymphangioblasts migrate dorsally and ventrally along trunk intersegmental arteries to form the ISLVs, TD, and DLLVs, which together establish the typical lymphatic network observed at 4–5 dpf[18–20]. In control larvae maintained in osmotic balanced condition, the lymphatic vasculature displayed the expected lymphatic network patterns, including ISLVs, TD, and DLLVs at 4 dpf (Fig. 3C), with a few remnants of the PLs still present along the horizontal myoseptum (Fig. 3D,E).

In edematous larvae, the typical lymphatic structures were observed, but with an additional increase in PLs, which were significantly expanded in edematous larvae (Fig. 3F–H). Quantitation of the PLs per 9 somites anterior to the urogenital pore revealed a two-fold increase in PLs in edematous larvae compared to controls (Fig. 3I). Importantly, the increase in PLs was not accompanied by delays in the formation of ISLVs, TD, or

◀**Fig. 2**. Lymphatic vessel expansion during edema recovery. (**A**) Confocal image of osmotically balanced *Tg(mrc1a:egfp; kdrl:mcherry)* larvae illustrating the normal vascular network at 9 dpf. (**B**) Lymphatic vessels are pseudo-colored in green from panel (A) (**C**) Magnified image of the thoracic duct in panel (B) (**D**) Confocal image of recovered edema-free *Tg(mrc1a:egfp; kdrl:mcherry)* larvae illustrating the vascular network following edema resolution. (**E**) Lymphatic vessels are pseudo-colored in green from panel D, highlighting the excess lateral lymphatics and dilated thoracic duct. (**F**) Magnified image of the thoracic duct in panel E. (**G**) Quantification of the thoracic duct surface area in controls ($n = 14$) and edema-resolved larvae ($n = 19$). (**H**) Quantification of the number of DLLV nuclei in controls ($n = 7$) and edema-free larvae ($n = 5$) in *Tg(fli1a:nEGFP; lyve1b:dsRed)* background. (**I**) Comparison of the number of LL segments in 9 somites between controls ($n = 11$) and edema-free larvae ($n = 10$). (**J**) Quantification of the number of intersegmental lymphatic vessels in controls ($n = 7$) and edema-free larvae ($n = 5$). (**K**) Confocal image of the facial lymphatics of osmotically balanced larvae at 9 dpf. (**L**) Lymphatic vessels are pseudo-colored in green from panel K. (**M**) Magnified image from panel L. (**N**) Confocal image of the facial lymphatics of recovered edema-free larvae at 9 dpf. (**O**) Lymphatic vessels are pseudo-colored in green from panel N. (**P**) Magnified image from panel O showing excessive lymphatic sprouts. (**Q**) Comparison of the total facial lymphatic area in controls ($n = 7$) and edema-free larvae ($n = 5$). (**R**) Number of facial LEC nuclei in controls ($n = 5$) and edema-free larvae ($n = 5$). *Tg(fli1a:nEGFP; lyve1b:dsRed)* was used for quantitation. Scale bar = 50 µm (A-L). $^{*}p < 0.05$, $^{**}p < 0.01$; $^{****}p < 0.0001$.

DLLVs, suggesting that edema promotes lymphangiogenesis rather than delaying its development (Fig. 3F,J). The number of PLs remained unchanged in the hypertonic solution between 48 and 72 hpf, suggesting that hypertonic stress does not lead to an increase in PLs (Supplementary Fig. 2A, B). However, an increase in the number of PLs was observed as early as 80 hpf with no difference in TD formation between unchallenged and osmotic-challenged fish, indicating that osmotic stress-induced edema acts as a stimulus to activate lymphangiogenesis (Supplementary Fig. 2C, D).

To examine endothelial cell changes during edema recovery, we used the *Tg(fli1a;nEGFP; lyve1b:dsRed)* transgenic line, which labels LEC nuclei within the lymphatic vasculature (Fig. 3K–N). At 8 dpf, edema-free larvae exhibited a significant increase in LEC numbers in the enlarged TD compared to controls (Fig. 3K–N). Quantitative analysis showed a 1.5-fold increase in LEC numbers in edema-free larvae (Fig. 3O). Endothelial hyperplasia was also observed in the posterior cardinal vein (PCV) of edema-free larvae, suggesting that edema may have activated pathways in other vascular beds (Fig. 3P). We also observed significant elongation of LEC nuclei in edema-free larvae compared to controls (Fig. 3K–N). Interestingly, stretching of EC nuclei was observed only in LECs on the thoracic duct but not in the blood endothelial cells (BECs) in the adjacent PCV (Fig. 3Q). These findings suggest that edema activates an extensive pro-angiogenic program, including lymphangiogenesis and endothelial cell remodeling.

We investigated whether PLs or facial lymphatics at the pre-edema stage could serve as indicators for edema outcomes to predict recovery. At 3 dpf, we analyzed the number of PLs at pre-edema stage, then applied an osmotic challenge at 4 dpf, induced edema at 5 dpf, and assessed recovery at 7 dpf (Supplementary Fig. 3A). The progression of edema development and recovery was monitored in 48 individual larvae. We found no association between the number of PLs and edema recovery (Supplementary Fig. 3B). Similarly, an evaluation between the facial lymphatics at 3 dpf showed no clear link between their pre-edema state and edema outcomes (Supplementary Fig. 3C). Therefore, neither PLs nor facial lymphatics serve as predictors for edema recovery. These findings suggest that edema outcomes are not determined by pre-edema status, and that the lymphatic enrichment program is activated during edema development.

Endothelial translatome in edema-driven lymphangiogenesis

To explore the molecular changes underlying edema-driven lymphangiogenesis in vivo, we employed Translating Ribosome Affinity Purification (TRAP) to isolate ribosome-bound mRNA from endothelial cells (Fig. 4). We generated a novel *Tg(mrc1a:egfp-2a-rpl10a3xHA)* transgenic line by using the mrc1a promoter sequence to drive the expression of an eGFP-2 A-rpl10a-3xHA transgene cassette[20]. This construct consists of eGFP, which is coexpressed with the 60 S ribosomal protein L10a (rpl10a) via a viral 2A peptide linkage, and the rpl10a is tagged with three hemagglutinin (HA) epitope sequences. This allows for the simultaneous visualization of transgene expression and translatome collection (Supplementary Fig. 4A). The "mrc1a:RiboTag" transgenic line is stably expressed in lymphatics and primitive veins, similar to the previously generated *Tg(mrc1a:egfp)*^{y251} line (Supplementary Fig. 4B)[20].

Using a *Tg(mrc1a:egfp-2a-rpl10a-3xHA)* transgenic line, we analyzed lymphatic and venous endothelial translatomes. We performed TaqMan qRT-PCR to confirm the enrichment lymphatic and primitive venous endothelial mRNAs. Gene expression analysis revealed significant enrichment of *flt4* (also known as *vegfr3*) and *lyve1b*, both of which are known to be expressed in lymphatics and primitive veins at this developmental stage. These results indicate the efficiency of the mrc1a: RiboTag transgenic line and the TRAP protocol for analyzing the endothelial translatome (Supplementary Fig. 4C). The ubiquitous gene Nedd4 binding protein 1 *(n4bp1)* showed no differences in expression between endothelial and non-endothelial mRNA, confirming the specificity of this assay for lymphatic and primitive vein endothelial cells (Supplementary Fig. 4C). Since mrc1a is also expressed in a subset of macrophages, we assessed whether the TRAP protocol enriched for a macrophage marker Mpeg1.1. Analysis of *mpeg1.1* revealed no differences in expression between endothelial and non-endothelial RNA samples, further confirming the endothelial specificity of this TRAP assay with minimal influence from the macrophage population (Supplementary Fig. 4C).

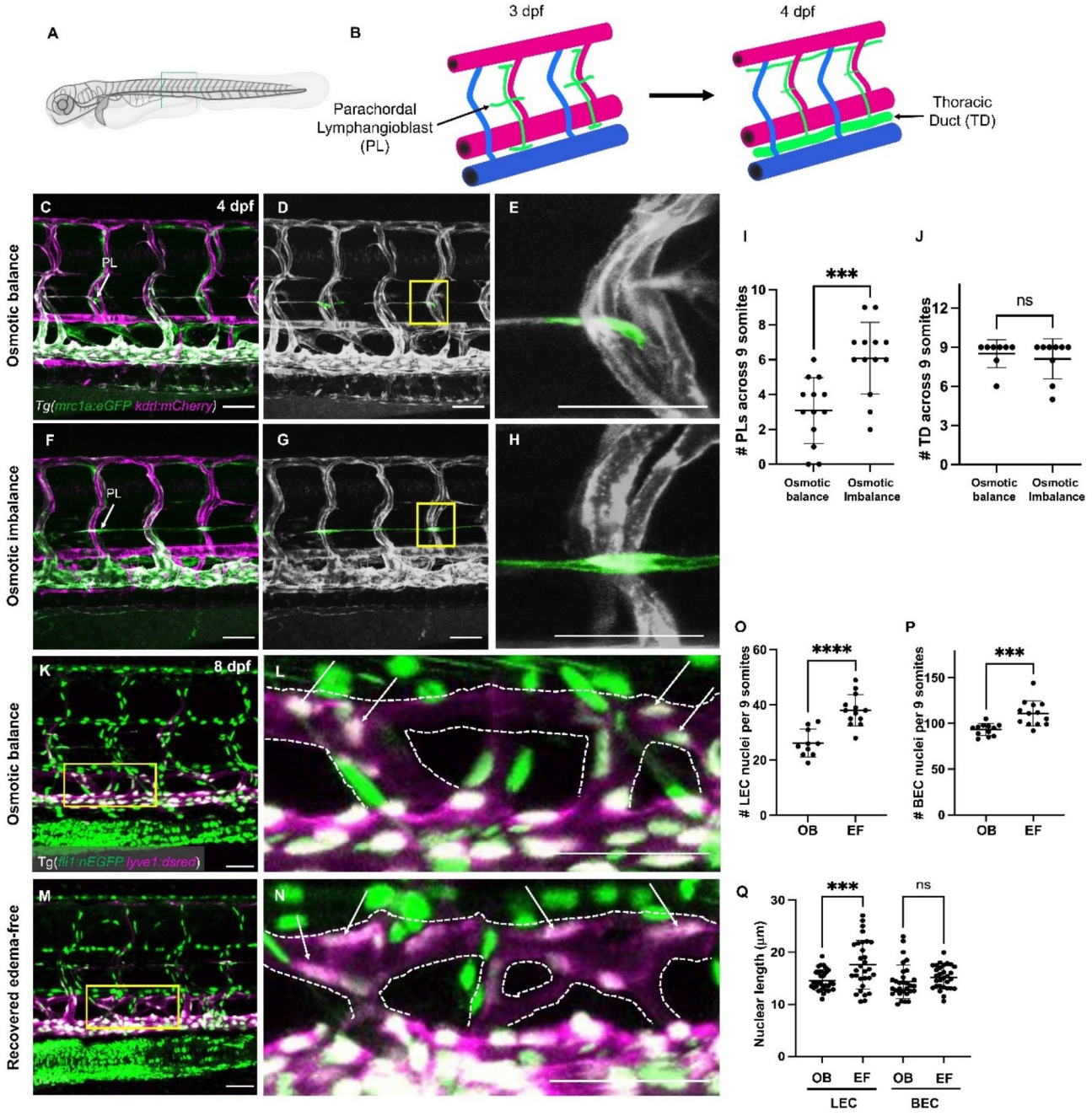

Control and edema-induced larvae were collected at 4 dpf, homogenized to obtain crude lysates, and the TRAP protocol enriched for endothelial mRNA by purifying the HA-tagged ribosomes using anti-HA antibody (Fig. 4A,B). The control non-endothelial RNAs were collected from the supernatant containing untagged ribosome-bound RNAs (Fig. 4A). Gene expression analysis showed that key endothelial markers, including *flt4*, *kdrl*, *and lyve1b*, were significantly upregulated in edematous larvae compared to controls (Fig. 4C). Although *prox1a* levels showed an upward trend, this was not statistically significant, and *vegfc* levels remained unchanged. To explore the contribution of other sources of vegf ligands, we isolated RNA from osmotic-stressed whole embryos and performed qPCR to assess the expression of *vegf* ligands relative to osmotic balance controls. Transcriptomic analysis of whole embryos revealed changes in *vegf* ligands during edema induction. Specifically, *vegfc* was upregulated, while *vegfd* was downregulated, suggesting a potential shift in Vegf signaling during edema (Supplementary Fig. 5A-C). No changes were observed in *vegfaa* expression levels (Supplementary Fig. 5A-C). These data highlight that edema acts as a potent activator of the lymphangiogenic program, driving gene expression changes in endothelial cells that facilitate the formation of new lymphatic vessels.

Role of Vegfr-dependent lymphangiogenesis in edema resolution

To investigate the necessity of lymphangiogenesis activation for edema recovery, we inhibited the lymphangiogenic program using Vegfr inhibitors. Vegfr3 signaling pathway is essential for both developmental and post-natal lymphangiogenesis[34,35]. Similar to mammals, zebrafish Vegfr3 signaling facilitates secondary sprouting from the

Fig. 3. Lymphatic endothelial cell proliferation and elongation during edema recovery. (**A**) Schematic illustrating the imaging area of trunk lymphatics. (**B**) Diagram of developmental steps of lymphatic progenitors that give rise to lymphatic vessels at 3–4 dpf. (**C**) Confocal image of osmotically balanced *Tg(mrc1a:egfp; kdrl:mcherry)* larvae showing normal vascular network at 4 dpf. (**D**) Pseudo-colored confocal micrograph of untreated transgenic larvae indicating the parachordal lymphangioblasts (PLs) in green and other vessels in grayscale. (**E**) Magnified image of the PLs in panel D. (**F**) Confocal image of osmotically imbalanced *Tg(mrc1a:egfp; kdrl:mcherry)* larvae showing the vascular phenotype in edema state. (**G**) Pseudo-colored confocal micrograph of osmotically imbalanced larvae highlighting the excess PLs during edema. (H) Magnified image of PL in panel F. (**I**) Quantification of the somites containing PLs. 9 somites per larvae were counted ($n = 13$ embryos each). (**J**) Comparison of the number of somites with TD fragments during edema formation at 4 dpf ($n = 9$ embryos each). (**K**) Confocal image of trunk vessels of an osmotically balanced *Tg(fli1:nEGFP; lyve1b:dsRed)* double transgenic larva. (**L**) Magnified image of the thoracic duct illustrating the oval-shaped LEC nuclei in panel K. The dotted lines indicate the boundary of the thoracic duct, and the arrows indicate LECs on the thoracic duct. (**M**) Confocal image of trunk vessels of a recovered edema-free *Tg(fli1:nEGFP; lyve1b:dsRed)* larva. (**N**) Magnified image of the thoracic duct highlighting the elongated LEC nuclei (arrow) in panel M. (**O**) Quantification of LECs in the thoracic duct of 9 somites between osmotic balanced ($n = 10$) and edema-free larvae ($n = 13$). (P) Quantification of BECs in the PCV across 9 somites between osmotic balanced ($n = 11$) and edema-free larvae ($n = 13$) (**Q**) Quantification of lymphatic or blood endothelial nuclei length in osmotically balanced or edema-resolved larvae. A total of 30 nuclei were counted from each group. Scale bar = 50 µm (A-H and J-M). ns, not significant; $^{***}p < 0.001$, $^{****}p < 0.0001$.

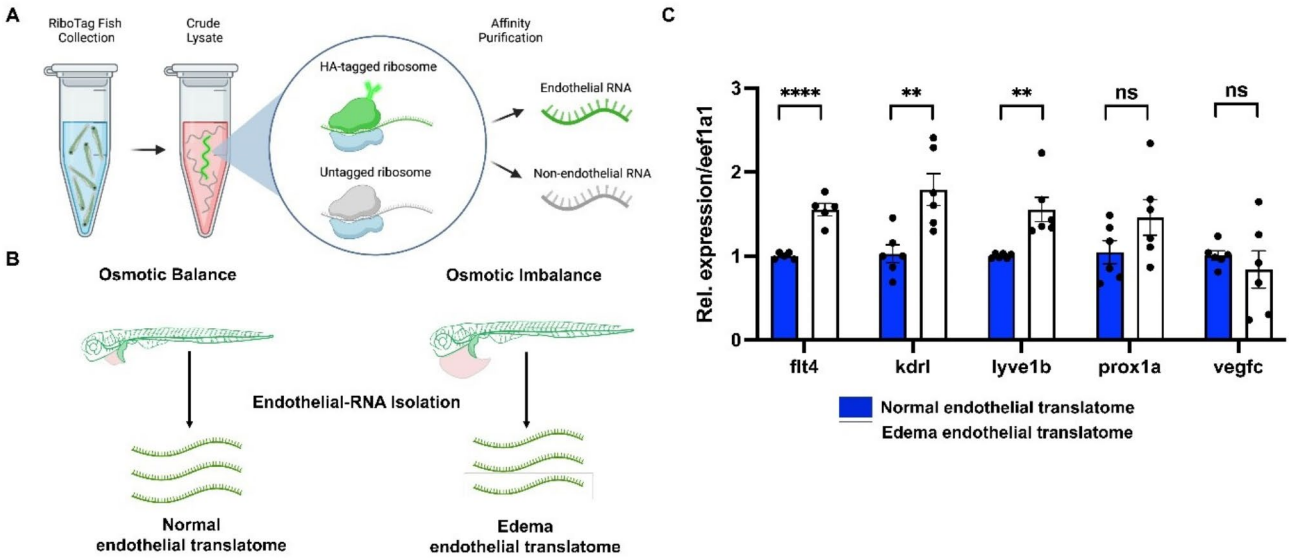

Fig. 4. Endothelial translatome analysis reveals upregulation of lymphangiogenic factors in edematous vessels. (**A**) Schematic of the experimental flow of translating ribosome affinity purification (TRAP) protocol to isolate endothelial and non-endothelial translatome. (**B**) The experimental design to analyze endothelial translatome from osmotically balanced and imbalanced edematous Ribotag transgenic fish using TRAP assay. (**C**) Comparison of the translatome analysis of key lymphatic genes in osmotically balanced and imbalanced edematous larvae. Each RNA sample was obtained from a pool of at least 350 embryos. ns, not significant; $^{**}p < 0.01$; $^{****}p < 0.0001$.

posterior cardinal vein to form lymphatic progenitors on the horizontal myoseptum, which migrates ventrally to establish the thoracic duct[18,19]. To specifically test the compensatory role of the lymphatics in edema clearance and disrupt lymphangiogenesis at the precise targeted time, we used Vegfr pathway inhibitors SAR131675[36–41] and SKLB1002[41–45]. Our dose-response assay using serial dilutions of the inhibitors at 48 hpf identified 10 µM SAR131675 and 5 µM SKLB1002 as the lowest effective dose (Supplementary Fig. 6). Additionally, we used difluorobenzocurcumin (CDF)[46], a potent anti-lymphangiogenic agent that has been shown to selectively inhibit the Vegfc-Vegfr3-ERK-signaling pathway in zebrafish. Treatment of 2.5 µM CDF significantly disrupted the development of trunk and facial lymphatic growth in zebrafish larvae (Supplementary Fig. 7). The inhibitors were treated at 48 hpf for 24 h when active lymphatic development initiates (Fig. 5A). Compared to the control group incubated in 0.1% DMSO, the larvae exposed to Vegfr inhibitors displayed edema fluid buildup (Fig. 5B). The precise timing of inhibitor treatment at 48 hpf was critical since the approach was to target the emergence of lymphatic progenitors and lymphangiogenesis without largely affecting angiogenesis. Treatment of 10 µM SAR131675 at earlier stage (e.g., 22 hpf) paused angiogenic sprouting (Supplementary Fig. 8A). All primary and secondary sprouting events in the trunk were ceased (Supplementary Fig. 8B-E). Similarly, not only lymphatic

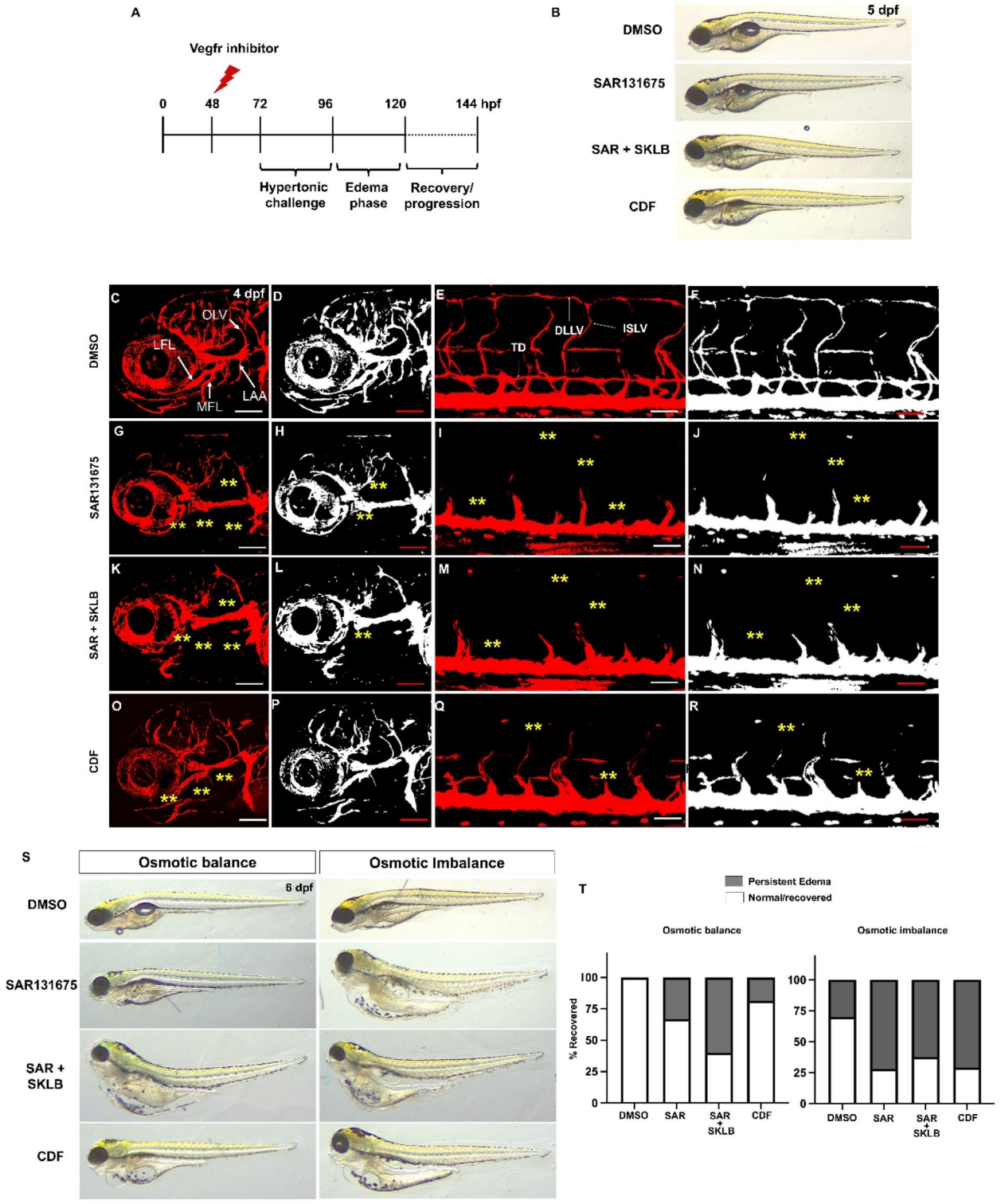

vessels but also blood vessels in the craniofacial area paused sprouting immediately after SAR131675 inhibitor treatment (Supplementary Fig. 8F-I). Delayed treatment of Vegfr inhibitor at 78 hpf caused cease the following lymphangiogenesis in the trunk and craniofacial area (Supplementary Fig. 9A). The larvae exposed to inhibitor treatments at 78 hpf, unlike the ones exposed at 48 hpf, did not form edema without exposure to osmotic stress (Supplementary Fig. 9B). Compared to the DMSO-treated larvae (Supplementary Fig. 9C-F), SAR131675-treated larvae showed defects in trunk lymphatics as they failed to form TD or DDLV (Supplementary Fig. 9G, H). Their craniofacial lymphatics were partially affected with stunted MFL and OLV, some changes in the LAAs, and unchanged LFL (Supplementary Fig. 9I, J). Combined SAR131675 and SKLB1002 treatment showed a stronger effect on preventing craniofacial lymphatics as MFL, OVL, and LAA were defective, but LFL remained largely unaffected (Supplementary Fig. 9K-N). At 78 hpf, the larvae already formed a large portion of LFL due to its developmental timing prior to the inhibitor treatments (Supplementary Fig. 10)[22,33]. Intriguingly, despite

◀**Fig. 5**. Vegfr-dependent lymphangiogenic program is required for edema fluid clearance. (**A**) Schematic diagram illustrating the experimental design for Vegfr inhibition during the osmotic challenge and edema progression. (**B**) Representative brightfield images showing edema formation in 5 dpf larvae treated with DMSO, 10 µM SAR131675, SAR131675 and 5µM SKLB1002 combined, 2.5 µM CDF in osmotically balanced conditions. (**C**) Confocal image of craniofacial vessels of a DMSO-treated *Tg(lyve1b:dsRed)* larva raised in an osmotically balanced condition. (**D**) Grayscale confocal micrograph of a DMSO-treated larva highlighting the facial lymphatics. (**E**) Confocal image of trunk vessels of a DMSO-treated *Tg(lyve1b:dsRed)* larva raised in an osmotically balanced condition. (**F**) Grayscale confocal micrograph of a DMSO-treated larva highlighting the thoracic duct. (**G**) Confocal image of craniofacial vessels of a SAR131675-treated *Tg(lyve1b:dsRed)* larva showing absence of facial lymphatics. (**H**) Grayscale confocal micrograph of a SAR131675-treated larva highlighting the complete loss of facial lymphatics (**I**) Confocal image of trunk vessels of a SAR131675-treated *Tg(lyve1b:dsRed)* larva showing complete absence of thoracic duct. (**J**) Grayscale confocal micrograph of a SAR131675-treated larva highlighting the loss of thoracic duct. (**K**) Confocal image of craniofacial vessels of a SAR131675 and SKLB1002 -treated *Tg(lyve1b:dsRed)* larva showing absence of facial lymphatics. (**L**) Grayscale confocal micrograph of a SAR131675 and SKLB1002-treated larva highlighting the loss of facial lymphatics (**M**) Confocal image of trunk vessels of a SAR131675 and SKLB1002 -treated *Tg(lyve1b:dsRed)* larva showing complete absence of thoracic duct. (**N**) Grayscale confocal micrograph of a SAR131675 and SKLB1002 -treated larva highlighting the loss of thoracic duct. (**O**) Confocal image of craniofacial vessels of a CDF-treated *Tg(lyve1b:dsRed)* larva showing partial absence of facial lymphatics. (**P**) Grayscale confocal micrograph of CDF-treated larva highlighting the partial loss of facial lymphatics (**Q**) Confocal image of trunk vessels of CDF-treated *Tg(lyve1b:dsRed)* larva showing significant disruption of thoracic duct development. (**R**) Grayscale confocal micrograph of CDF-treated larva highlighting the loss of thoracic duct. (**S**) Representative brightfield images showing edema outcomes in 6 dpf larvae treated with DMSO, SAR131675, SAR131675 and SKLB1002 combined, or CDF in osmotically balanced or imbalanced conditions. (**T**) The percentage of edema recovery demonstrated by the ratio of larvae recovered from edema or developed persistent edema at 8 dpf under DMSO and inhibitor treatments in osmotic balance and osmotic imbalance conditions. LFL, Lateral facial lymphatics; MFL, Medial facial lymphatics; LAA, Lymphatic brachial arches; OLV, Otholitic lymphatic vessels. Yellow asterisks indicate missing lymphatic structures in panels F-M. Scale bars = 500 µm (**B**), 50 µm (**C**-**R**).

inhibition of the Vegf pathway starting at 78 hpf and continuing until 9 dpf (Supplementary Fig. 11A), edema did not form without osmotic challenge (Supplementary Fig. 11B). Although delayed inhibitor treatments significantly reduced lymphatic vessel growth of both trunk and facial lymphatics, remanent lymphatics that formed prior to inhibitor treatment was sufficient to maintain steady state (Supplementary Fig. 11C-S). This data reconfirms how using Vegfr inhibitors can precisely inhibit lymphatic vessel growth in a highly time-sensitive manner.

Disruption of lymphangiogenesis impairs edema clearance

While Vegfr3 is a key player in lymphangiogenesis, some lymphatic vessel beds also demand Vegfr2, particularly in the zebrafish craniofacial lymphatics[47]. Vegfr2 is required for proper craniofacial lymphatic development and has been shown to compensate for *vegfr3* haplo-insufficiency in lymphangiogenesis[47]. Thus, in addition to Vegfr3 inhibition, we used 5 µM of SKLB1002 to inhibit Vegfr2, preventing possible compensation for incomplete Vegfr3 inhibition. The control group (DMSO) displayed normal craniofacial and trunk lymphatic vessel phenotypes at 5 dpf as expected (Fig. 5C–F). However, larvae treated with SAR131675 failed to form the craniofacial and trunk lymphatics (Fig. 5G–J). The facial lymphatics lacked all major lymphatic structures, including LFL, MFL, OLV, and LAA (Fig. 5G,H) as well as the trunk lymphatics such as TD, ISLV, and DLLV (Fig. 5I,J). Similarly, a combination of SAR131675 and SKLB1002 disrupted the craniofacial and trunk lymphatics (Fig. 5K–N). Following CDF treatment, we observed significant loss of trunk and facial lymphatic structures. The CDF-treated larvae revealed complete loss of MFL and LAA and stunting of the LFL and OLV (Fig. 5O,P) together with massive depletion of the TD and DLLV in the trunk (Fig. 5Q,R). Inhibition of lymphangiogenesis resulted in edema in osmotically balanced environment and the severity elevated in osmotic imbalanced environment at 6 dpf (Fig. 5S). Two days later, at 8 dpf, in an osmotically balanced environment, 67% (SAR131675 alone), 40% (SAR131675 and SKLB1002) and 81% (CDF) of larvae restored fluid balance and became edema-free (Fig. 5T). Note that although 24 h of Vegfr inhibitor treatments (48 to 72 hpf) effectively inhibited lymphangiogenesis (Fig. 5), lymphangiogenesis is rescued in the later stages in the edema-free larvae (Supplementary Fig. 12), and inherently enhanced by the edema-induced compensatory lymphangiogenesis (Figs. 2 and 3). In contrast, in an osmotically imbalanced condition, where the experimental setting at 70% of DMSO-treated larvae became edema-free, the inhibitor-treated groups displayed a significant decrease of the edema recovery rate (Fig. 5T). The recovery rate significantly dropped to 28%, 38%, and 29% in the groups treated with SAR131675, combination of SAR131675 and SKLB1002, and CDF, respectively (Fig. 5T). Similarly, when lymphatic growth was partially inhibited by delayed treatment starting from 78 hpf, all larvae were unable to recover from induced edema without the rescue of lymphatic vessels (Supplementary Fig. 11O, P).

We analyzed the lymphatics of edema-free larvae from two groups raised under osmotically balanced or imbalanced conditions (Supplementary Fig. 12A). Both groups were treated with Vegfr inhibitors at 48 hpf for 24 h (Fig. 5A), and larvae that had recovered from edema by 8 dpf were analyzed (Fig. 5T, Supplementary Fig. 12A). Notably, larvae that developed edema at 5–6 dpf due to loss of lymphatics largely re-established their lymphatic structures by 8 dpf and regained the ability to clear excess fluid (Supplementary Fig. 12). All edema-

free larvae exhibited robust recovery of craniofacial lymphatics in both groups, regardless of osmotic or inhibitor conditions (Supplementary Fig. 12B, D,F, H,J, L,N, P), while trunk lymphatics showed partial and somewhat variable recovery (Supplementary Fig. 12C, E,G, I,K, M,O, Q). In contrast, larvae unable to reconstruct their lymphatic structures failed to recover, continued to develop severe edema, and eventually died. These findings suggest that craniofacial lymphatics play a critical role in fluid regulation at this developmental stage, and that edema promotes the expansion of the lymphatic network, further supporting the role of edema in enhancing lymphangiogenesis in zebrafish. Together, these results underscore the essential role of lymphatics in fluid clearance and edema reduction in zebrafish larvae.

Discussion

In this study, we investigated the mechanisms underlying the resolution of edema in zebrafish larvae, with a particularly focus on the role of the lymphatic system in fluid clearance. Our findings highlight that lymphatic vessel remodeling, particularly in the craniofacial and trunk regions, plays a key role in edema fluid clearance. This process is driven by Vegfr-dependent lymphangiogenesis, suggesting that the formation of new lymphatic vessels in response to fluid accumulation is essential for edema resolution.

Our results support the critical role of compensatory lymphangiogenesis in resolving edema. The rapid expansion of lymphatic vessels observed in our experiments is consistent with previous studies demonstrating the central role of the lymphatic system in maintaining fluid homeostasis during interstitial fluid accumulation[12–15]. Lymphatic vessel expansion facilitates fluid drainage, helping restore normal fluid balance and reduce swelling[1,48]. The importance of lymphangiogenesis in edema resolution is further emphasized by our observation of increased VEGFR signaling following osmotic stress. This finding aligns with studies showing that VEGFR-3 signaling is crucial for lymphatic endothelial cell proliferation and vessel sprouting, processes necessary for the development of new lymphatic vessels[35,49].

Our edema-induction model provides a reproducible and quantifiable system for studying edema formation. Given that a single pair of zebrafish breeders can produce 200–300 eggs, this approach offers a statistically robust experimental framework[50]. Our model demonstrates a robust and reproducible edema formation, with distinct swelling patterns in body parts. The use of brightfield time-lapse imaging provided high-resolution visualization of edema progression, revealing that edema formation was both time-dependent and tissue-specific, with the pericardial cavity swelling first, followed by the yolk, and eventually the whole body when fluid clearance fails. This aligns with findings in other species, where the pericardial region is often on of the first sites to exhibit fluid accumulation due to its proximity to the heart, a key organ in maintaining osmotic balance[51–53].

This model also aligns with the timeline of natural lymphatic development, as lymphatic progenitors emerge around 2 dpf and subsequently proliferate and migrate to their designated locations[18–20]. Complete edema recovery is observed within 48 h post-osmotic stress exposure, coinciding with the expansion of the lymphatic network. However, precisely distinguishing normal development processes from additional lymphatic expansion during this period is challenging due to overlapping biological pathways. Both developmental and regenerative vascular processes involve the activation of lymphangiogenic programs and growth factors like Vegf and their receptors[54]. In zebrafish, the rapid expansion of lymphatic vessels in response to edema closely resembles developmental processes, complicating the efforts to separate the two. More refined models or markers are needed to distinguish these stages and enable precise temporal and spatial dissection of these processes in vivo.

While studies in rodents have shown that long-term high-salt diets (~2 weeks) promote lymphangiogenesis through macrophage-secreted Vegfc and Vegfr3 signaling[55–57], neither short-term (24 h) nor extended (48 h) hypertonic stress exposure in our study altered lymphangiogenesis (Supplementary Fig. 2). This suggests that it is the fluid accumulation, rather than the salt treatment itself, that triggered the lymphangiogenic response. Our findings are consistent with those from ex vivo mouse embryos, where forced fluid injection activates lymphatic endothelial cells (LEC) and promotes lymphatic vessel expansion[48], underscoring an evolutionarily conserved mechanism for lymphatic activation and fluid drainage. While lymphatic expansion has been linked to the expression of Vegfc and matrix metalloproteinases[58], the precise causal relationship between these signals and the generation of *de novo* LECs and functional lymphatic vessels capable of clearing edema remains to be fully elucidated.

Further insights into the dynamic process of lymphangiogenesis were provided by high-resolution intravital live imaging in zebrafish. This model enabled detailed analysis lymphatic progenitor cell generation and extensive remodeling of lymphatic vessels during edema recovery. While various animal models have been developed to study the role of lymphatic vessels in fluid drainage and edema clearance[59,60], traditional models often lack the spatial and temporal resolution needed to capture lymphatic changes comprehensively[60–62]. Live imaging in zebrafish allows real-time observation of the dynamic processes involved in lymphangiogenesis, providing valuable insights into their regulatory mechanisms throughout edema progression.

Restoration of craniofacial and trunk lymphatics is essential for edema clearance. When larvae failed to restore lymphatic structures, fluid drainage was impaired, and edema progression continued. Our data also highlight that although lymphatic remodeling occurs spontaneously throughout the body in response to edema, craniofacial lymphatics play a critical role in fluid clearance during these developmental stages[63]. While the specific stimulus that activates the lymphangiogenic program during edema progression remains unidentified, pathways involved in inflammation may have contributed to lymphangiogenesis[64], as there is marked increase of neutrophils and macrophages in edematous larvae (Supplementary Fig. 13). Increased interstitial pressure from fluid accumulation suggests that pressure-sensitive sensors, such as Piezo1/2 or members of the *Trpc* family, and mechanotransduction signaling may be involved.

A unique aspect of our study was the use of Translating Ribosome Affinity Purification (TRAP) to capture endothelial-specific gene expression during edema resolution. This technique isolates ribosome-bound mRNAs undergoing active translation from specific cell types or tissues in vivo, thereby circumventing the cell dissociation

steps that could disrupt cell identity and alter gene expression[65,66]. As a result, TRAP provides an accurate 'in vivo snapshot' of molecular changes in specific cell populations[67–69]. Our TRAP approach provided valuable insights into the transcriptional landscape of endothelial cells during edema resolution and will be useful for future studies exploring the genetic regulation of lymphangiogenesis. The mrc1a promotor used in this study drives expression in lymphatics, primitive veins, and a subset of macrophages[20]. As a result, identifying the pure lymphatic translatome remains a limitation, as this promoter does not exclusively label lymphatic endothelial cells. The combined use of the mrc1a: RiboTag transgenic line with recently developed enhancer lines could potentially enhance the molecular resolution of the lymphatic translatome[70,71].

In conclusion, this study underscores the importance of compensatory lymphangiogenesis in the resolution of edema and the restoration of fluid homeostasis. The rapid expansion of lymphatic vessels, driven by Vegfr3 signaling plays a critical role in alleviating edema and restoring normal fluid balance in tissues. These findings enhance our understanding of the molecular mechanisms regulating lymphatic function in the context of edema and highlight lymphangiogenesis as a potential therapeutic target for conditions characterized by fluid retention. Future research should aim to further elucidate the molecular mechanisms underlying compensatory lymphangiogenesis, particularly how different signaling pathways coordinate lymphatic vessel response and fluid clearance. By advancing our understanding of these processes, we may be able to develop more effective therapies for diseases associated with fluid retention and impaired lymphatic function.

Methods

Zebrafish maintenance and fish strains

Zebrafish husbandry and research protocols were approved by the University of Illinois Animal Care and Institutional Biosafety Committee (Animal Care and Use Protocol 23–112). All procedures adhered to relevant guidelines and regulations, conforming to the ARRIVE guidelines[72]. Zebrafish embryos were obtained through natural spawning and raised in blue egg water (60 ug/ml of Instant Ocean and 0.0001% methylene blue) at 28.5 °C under standard conditions. For imaging vascular morphology, we used the *Tg(mrc1a:egfp; kdrl:mCherry)* double transgenic line[20]. *Tg(fli1:nEGFP; Tg(lyve1b:dsRed)* and *Tg(mrc1a:nls-egfp; Tg(lyve1b:dsRed)* double transgenic line was used for the quantification of endothelial cell (LEC) numbers[18,22]. *Tg(mrc1a:egfp-2A-rpl10a-3xHA)* was generated in this study and employed for isolating the endothelial translatome for quantitative PCR analysis. *Tg(lyz:dsRed)*[73] and *Tg(mpeg1:mCherry)*[74] were used for neutrophil and macrophage measurement, respectively. Ekkwill strain were used for the study.

Induction of edema with osmotic stress

Embryos were dechorionated at 48 hpf either manually or using a 1 mg/mL pronase (Sigma-Aldrich) in blue water for 2–5 min, followed by gentle pipetting. After dechorionation, embryos were washed three times in fresh blue water to remove any residual pronase. Dechorionated embryos were incubated in a hypertonic salt solution (3x Danieau buffer: 58 mM NaCl, 0.7 mM KCl, 0.4 mM $MgSO_4$, 0.6 mM $Ca(NO_3)_2$, 10 mM HEPES) with an osmolarity of 375 mOsm/L for 24 h. They were then returned to a isotonic solution (0.3x Danieau buffer, 37.5 mOsm/L). This osmotic stress protocol consistently induced reproducible edema, which was quantified using the freehand selection tool in ImageJ to trace the body region boundaries in lateral view at designated developmental stages. The edema surface area was measured in pixels. Confocal image analyses were performed across nine somitic segments rostral to the urogenital pore, counting the number of somites containing lymphatics.

Lymphangiogenesis inhibitors

To assess the effect of Vegfr inhibitors on blood and lymphatic vessel formation during edema, larvae were treated with the SAR131675[36] (Selleck Chemicals), SKLB1002[42] (Selleck Chemicals), 4-(3,4-Diflurobenzo) curcumin (Cayman Chemicals), or 0.1% DMSO (as control) at indicated time points. After the treatments, the larvae washed out and subjected to osmotic stress starting at 3 dpf. In an alternate treatment strategy, larvae were first exposed to osmotic stress from 3 dpf, followed by Vegfr inhibitor treatment at designated time points and incubation up to 5 dpf. The inhibitors were washed out at 5 dpf, and vascular changes during edema progression and resolution were quantified. For prolonged treatment, the drug was refreshed daily, and vascular changes were assessed at 9 dpf.

Generation of ribotag construct and Transgenic lines

The RiboTag construct was generated using Tol2kit components in combination with Gateway Technology[75]. To create the mrc1a:eGFP-2A-rpl10a-3xHA DNA construct, we recombined p5E-mrc1a promoter[20], pME-eGFP-2A-rp110a-3xHA[66], and p3E-polyA[75] into pDestTol2pA2[75] using LR clonase II (Thermo Fisher Scientific). The resulting DNA construct was co-injected with Tol2 transposase RNA into one-cell stage zebrafish embryos. A stable *Tg(mrc1a:egfp-2a-rpl10a-3xHA)* transgenic line was established after screening over multiple generations. This transgenic line effectively isolates the active lymphatic and venous endothelial translatome at desired developmental stages.

Translating ribosome affinity purification (TRAP)

TRAP was performed using a modified protocol[66]. For each untreated or edematous sample, 500 larvae were deyolked and homogenized in homogenization buffer composed of 1 mM Tris pH 7.4, 100 mM KCl, 12 mM $MgCl_2$, 1% NP-40, 1 mM DTT, 1x Protease inhibitors (Sigma), 200 units/mL RNAsin (Promega), 100ug/mL cycloheximide (Sigma) and 1 mg/mL heparin (Sigma). Lysates were incubated on ice for cell lysis and then cleared by centrifugation 10,000 x g for 10 min at 4 °C. Anti-HA antibody (2 µl, Abcam ab9110 Rabbit polyclonal) was added to 500 larvae equivalents in 800 µl lysate, followed by incubation on an orbital rotator at 4 °C for 4 h. Dynabeads® Protein G slurry (Novex/Life Technologies) was pre-washed with homogenization buffer and

incubated for 30 min to equilibrate the beads. After removal of the homogenization buffer, the lysate-antibody mixture was added to the beads and incubated overnight at 4 °C on an orbital rotator. Beads were collected using a magnetic stand and washed three times in high-salt homogenization buffer (50 mM Tris pH 7.4, 300 mM KCl, 12 mM $MgCl_2$, 1% NP-40, 1mM DTT, 1x Protease inhibitors, 200 units/mL RNAsin, 100ug/mL cyclohexamide, 1 mg/mL heparin) for 5 min per wash. Ribosome-bound RNA was retrieved from the beads and DNase-treated using the Direct-zol™ RNA MicroPrep kit (Zymo Research).

Image acquisition and processing

Embryos were anesthetized in 1x tricaine (MS-222) and subsequently mounted laterally or dorsally in 1% low-melting point agarose gel, on a 35 mm dish with a No. 1.5 coverslip and 14 mm glass diameter. Stereoscope images were captured using a Zeiss Stemi 305 microscope equipped with Axiocam Erc 5s camera (Zeiss) and an EVOS M5000 (ThermoFisher). Time-lapse videos of edema formation were recorded at a frame rate of 5 frames per second (fps) in MP4 format using the EVOS M5000. Confocal imaging was performed on a Zeiss LSM 880 confocal microscope, capturing high-resolution z-stack images with 10x or 20x objective lenses at a frame size of 1024 × 1024 pixels. The bi-directional image scanning speed was set to 7. Image analysis was performed using ImageJ (version: 2.3.0/1.53q) and Adobe Photoshop (Adobe).

Statistical analysis

All analyses were conducted using GraphPad Prism Software, version 9.2.0. The normality of all numerical datasets was tested with a Shapiro-Wilk test. An unpaired two-tailed Student's t-test was used for normally distributed data, and Mann-Whitney test was used if normality was not confirmed. Data are presented as mean ± standard deviation. Significance was defined as a p-value of less than 0.05.

Data availability

No datasets were generated or analysed during the current study.

Received: 16 May 2024; Accepted: 4 March 2025
Published online: 10 March 2025

References

1. Breslin, J. W. Edema and lymphatic clearance: Molecular mechanisms and ongoing challenges. *Clin. Sci. (Lond.)* **137**, 1451–1476. https://doi.org/10.1042/CS20220314 (2023).
2. Dongaonkar, R. M. et al. Edemagenic gain and interstitial fluid volume regulation. *Am. J. Physiol. Regul. Integr. Comp. Physiol.* **294**, R651-659. https://doi.org/10.1152/ajpregu.00354.2007 (2008).
3. Schrier, R. W. Pathogenesis of sodium and water retention in high-output and low-output cardiac failure, nephrotic syndrome, cirrhosis, and pregnancy (2). *N. Engl. J. Med.* **319**, 1127–1134. https://doi.org/10.1056/NEJM198810273191705 (1988).
4. Abassi, Z., Khoury, E. E., Karram, T. & Aronson, D. Edema formation in congestive heart failure and the underlying mechanisms. *Front. Cardiovasc. Med.* **9**, 933215. https://doi.org/10.3389/fcvm.2022.933215 (2022).
5. Oliver, G., Kipnis, J., Randolph, G. J. & Harvey, N. L. The lymphatic vasculature in the 21(st) century: Novel functional roles in homeostasis and disease. *Cell* **182**, 270–296. https://doi.org/10.1016/j.cell.2020.06.039 (2020).
6. Petrova, T. V. & Koh, G. Y. Biological functions of lymphatic vessels. *Science* **369**, eaax4063. https://doi.org/10.1126/science.aax4063 (2020).
7. Rutkowski, J. M., Boardman, K. C. & Swartz, M. A. Characterization of lymphangiogenesis in a model of adult skin regeneration. *Am. J. Physiol. Heart Circ. Physiol.* **291**, H1402-1410. https://doi.org/10.1152/ajpheart.00038.2006 (2006).
8. Beerens, M. et al. Multipotent adult progenitor cells support lymphatic regeneration at multiple anatomical levels during wound healing and lymphedema. *Sci. Rep.* **8**, 3852. https://doi.org/10.1038/s41598-018-21610-8 (2018).
9. Gur-Cohen, S. et al. Stem cell-driven lymphatic remodeling coordinates tissue regeneration. *Science* **366**, 1218–1225. https://doi.org/10.1126/science.aay4509 (2019).
10. Saaristo, A. et al. Vascular endothelial growth factor-C accelerates diabetic wound healing. *Am. J. Pathol.* **169**, 1080–1087. https://doi.org/10.2353/ajpath.2006.051251 (2006).
11. Hettrick, H. & Aviles, F. All edema is lymphedema: Progressing lymphedema and wound management to an integrated model of care. *Wound Manag. Prev.* **68**, 8–15 (2022).
12. Bates, D. O. An interstitial hypothesis for breast cancer related lymphoedema. *Pathophysiology* **17**, 289–294. https://doi.org/10.1016/j.pathophys.2009.10.006 (2010).
13. Yoon, Y. S. et al. VEGF-C gene therapy augments postnatal lymphangiogenesis and ameliorates secondary lymphedema. *J. Clin. Invest.* **111**, 717–725. https://doi.org/10.1172/JCI15830 (2003).
14. Szoke, D. et al. Nucleoside-modified VEGFC mRNA induces organ-specific lymphatic growth and reverses experimental lymphedema. *Nat. Commun.* **12**, 3460. https://doi.org/10.1038/s41467-021-23546-6 (2021).
15. Hartiala, P. et al. Phase 1 Lymfactin(®) study: Short-term safety of combined adenoviral VEGF-C and lymph node transfer treatment for upper extremity lymphedema. *J. Plast. Reconstr. Aesthet. Surg.* **73**, 1612–1621. https://doi.org/10.1016/j.bjps.2020.05.009 (2020).
16. Gemberling, M., Bailey, T. J., Hyde, D. R. & Poss, K. D. The zebrafish as a model for complex tissue regeneration. *Trends Genet.* **29**, 611–620. https://doi.org/10.1016/j.tig.2013.07.003 (2013).
17. Hogan, B. M. & Schulte-Merker, S. How to plumb a pisces: Understanding vascular development and disease using zebrafish embryos. *Dev. Cell* **42**, 567–583. https://doi.org/10.1016/j.devcel.2017.08.015 (2017).
18. Yaniv, K. et al. Live imaging of lymphatic development in the zebrafish. *Nat. Med.* **12**, 711–716. https://doi.org/10.1038/nm1427 (2006).
19. Kuchler, A. M. et al. Development of the zebrafish lymphatic system requires VEGFC signaling. *Curr. Biol.* **16**, 1244–1248. https://doi.org/10.1016/j.cub.2006.05.026 (2006).
20. Jung, H. M. et al. Development of the larval lymphatic system in zebrafish. *Development* **144**, 2070–2081. https://doi.org/10.1242/dev.145755 (2017).
21. Jung, H. M. et al. Imaging blood vessels and lymphatic vessels in the zebrafish. *Methods Cell Biol.* **133**, 69–103. https://doi.org/10.1016/bs.mcb.2016.03.023 (2016).
22. Okuda, K. S. et al. lyve1 expression reveals novel lymphatic vessels and new mechanisms for lymphatic vessel development in zebrafish. *Development* **139**, 2381–2391. https://doi.org/10.1242/dev.077701 (2012).
23. Das, R. N. et al. Generation of specialized blood vessels via lymphatic transdifferentiation. *Nature* **606**, 570–575. https://doi.org/10.1038/s41586-022-04766-2 (2022).

24. Jung, H. M. et al. MicroRNA-mediated control of developmental lymphangiogenesis. *eLife* **8**, e46007. https://doi.org/10.7554/eLife.46007 (2019).
25. Shin, M. et al. Valves are a conserved feature of the zebrafish lymphatic system. *Dev. Cell* **51**, 374–386. https://doi.org/10.1016/j.devcel.2019.08.019 (2019).
26. Castranova, D. et al. Live imaging of intracranial lymphatics in the zebrafish. *Circ. Res.* **128**, 42–58. https://doi.org/10.1161/CIRCRESAHA.120.317372 (2021).
27. Nicenboim, J. et al. Lymphatic vessels arise from specialized angioblasts within a venous niche. *Nature* **522**, 56–61. https://doi.org/10.1038/nature14425 (2015).
28. Boisen, A. M., Amstrup, J., Novak, I. & Grosell, M. Sodium and chloride transport in soft water and hard water acclimated zebrafish (Danio rerio). *Biochim. Biophys. Acta* **1618**, 207–218. https://doi.org/10.1016/j.bbamem.2003.08.016 (2003).
29. Barton, B. A. Stress in fishes: A diversity of responses with particular reference to changes in circulating corticosteroids. *Integr. Comp Biol.* **42**, 517–525. https://doi.org/10.1093/icb/42.3.517 (2002).
30. Flynt, A. S. et al. miR-8 microRNAs regulate the response to osmotic stress in zebrafish embryos. *J. Cell Biol.* **185**, 115–127. https://doi.org/10.1083/jcb.200807026 (2009).
31. Fiol, D. F. & Kultz, D. Osmotic stress sensing and signaling in fishes. *FEBS J.* **274**, 5790–5798. https://doi.org/10.1111/j.1742-4658.2007.06099.x (2007).
32. Singleman, C. & Holtzman, N. G. Growth and maturation in the zebrafish, Danio rerio: A staging tool for teaching and research. *Zebrafish* **11**, 396–406. https://doi.org/10.1089/zeb.2014.0976 (2014).
33. Eng, T. C. et al. Zebrafish facial lymphatics develop through sequential addition of venous and non-venous progenitors. *EMBO Rep.* **20**, e47079. https://doi.org/10.15252/embr.201847079 (2019).
34. Veikkola, T. et al. Signalling via vascular endothelial growth factor receptor-3 is sufficient for lymphangiogenesis in transgenic mice. *EMBO J.* **20**, 1223–1231. https://doi.org/10.1093/emboj/20.6.1223 (2001).
35. Karkkainen, M. J. et al. Vascular endothelial growth factor C is required for sprouting of the first lymphatic vessels from embryonic veins. *Nat. Immunol.* **5**, 74–80. https://doi.org/10.1038/ni1013 (2004).
36. Alam, A. et al. SAR131675, a potent and selective VEGFR-3-TK inhibitor with antilymphangiogenic, antitumoral, and antimetastatic activities. *Mol. Cancer Ther.* **11**, 1637–1649. https://doi.org/10.1158/1535-7163.MCT-11-0866-T (2012).
37. Espagnolle, N. et al. Specific inhibition of the VEGFR-3 tyrosine kinase by SAR131675 reduces peripheral and tumor associated immunosuppressive myeloid cells. *Cancers (Basel)* **6**, 472–490. https://doi.org/10.3390/cancers6010472 (2014).
38. Nihei, M. et al. Chronic inflammation, lymphangiogenesis, and effect of an anti-VEGFR therapy in a mouse model and in human patients with aspiration pneumonia. *J. Pathol.* **235**, 632–645. https://doi.org/10.1002/path.4473 (2015).
39. Hwang, S. D. et al. Inhibition of lymphatic proliferation by the selective VEGFR-3 inhibitor SAR131675 ameliorates diabetic nephropathy in db/db mice. *Cell Death Dis.* **10**, 219. https://doi.org/10.1038/s41419-019-1436-1 (2019).
40. Babaei, Z., Panjehpour, M., Parsian, H. & Aghaei, M. SAR131675 exhibits anticancer activity on human ovarian cancer cells through inhibition of VEGFR-3/ERK1/2/AKT signaling pathway. *Cell Signal* **111**, 110856. https://doi.org/10.1016/j.cellsig.2023.110856 (2023).
41. Kontarakis, Z., Rossi, A., Ramas, S., Dellinger, M. T. & Stainier, D. Y. R. Mir-126 is a conserved modulator of lymphatic development. *Dev. Biol.* **437**, 120–130. https://doi.org/10.1016/j.ydbio.2018.03.006 (2018).
42. Zhang, S. et al. SKLB1002, a novel potent inhibitor of VEGF receptor 2 signaling, inhibits angiogenesis and tumor growth in vivo. *Clin. Cancer Res.* **17**, 4439–4450. https://doi.org/10.1158/1078-0432.CCR-10-3109 (2011).
43. Shen, G. et al. SKLB1002, a novel inhibitor of VEGF receptor 2 signaling, induces vascular normalization to improve systemically administered chemotherapy efficacy. *Neoplasma* **59**, 486–493. https://doi.org/10.4149/neo_2012_062 (2012).
44. Yan, H. X., Wang, Y., Yang, X. N., Fu, L. X. & Tang, D. M. A new selective vascular endothelial growth factor receptor 2 inhibitor ablates disease in a mouse model of psoriasis. *Mol. Med. Rep.* **8**, 434–438. https://doi.org/10.3892/mmr.2013.1500 (2013).
45. Liu, Z., Qi, L., Li, Y., Zhao, X. & Sun, B. VEGFR2 regulates endothelial differentiation of colon cancer cells. *BMC Cancer* **17**, 593. https://doi.org/10.1186/s12885-017-3578-9 (2017).
46. Okuda, K. S. et al. 3,4-difluorobenzocurcumin inhibits Vegfc-Vegfr3-Erk signalling to block developmental lymphangiogenesis in zebrafish. *Pharmaceuticals (Basel)* **14**, 614. https://doi.org/10.3390/ph140706145 (2021).
47. Vogrin, A. J. et al. Evolutionary differences in the Vegf/Vegfr code reveal organotypic roles for the endothelial cell receptor Kdr in developmental lymphangiogenesis. *Cell Rep.* **28**, 2023–2036. https://doi.org/10.1016/j.celrep.2019.07.055 (2019).
48. Planas-Paz, L. et al. Mechanoinduction of lymph vessel expansion. *EMBO J.* **31**, 788–804. https://doi.org/10.1038/emboj.2011.456 (2012).
49. Jeltsch, M. et al. Hyperplasia of lymphatic vessels in VEGF-C transgenic mice. *Science* **276**, 1423–1425. https://doi.org/10.1126/science.276.5317.1423 (1997).
50. Hill, A. J., Teraoka, H., Heideman, W. & Peterson, R. E. Zebrafish as a model vertebrate for investigating chemical toxicity. *Toxicol. Sci.* **86**, 6–19. https://doi.org/10.1093/toxsci/kfi110 (2005).
51. Kojima, A. et al. A simple mouse model of pericardial adhesions. *J. Cardiothorac. Surg.* **14**, 124. https://doi.org/10.1186/s13019-019-0940-9 (2019).
52. Schwarz, E. R. et al. A small animal model of non-ischemic cardiomyopathy and its evaluation by transthoracic echocardiography. *Cardiovasc. Res.* **39**, 216–223. https://doi.org/10.1016/s0008-6363(98)00009-1 (1998).
53. Mauro, A. G. et al. The role of NLRP3 inflammasome in pericarditis: Potential for therapeutic approaches. *JACC Basic Transl. Sci.* **6**, 137–150. https://doi.org/10.1016/j.jacbts.2020.11.016 (2021).
54. Park, K. M. & Gerecht, S. Harnessing developmental processes for vascular engineering and regeneration. *Development* **141**, 2760–2769. https://doi.org/10.1242/dev.102194 (2014).
55. Karlsen, T. V. et al. High-salt diet causes expansion of the lymphatic network and increased lymph flow in skin and muscle of rats. *Arterioscler. Thrombosis Vasc. Biol.* **38**, 2054–2064. https://doi.org/10.1161/ATVBAHA.118.311149 (2018).
56. Machnik, A. et al. Macrophages regulate salt-dependent volume and blood pressure by a vascular endothelial growth factor-C-dependent buffering mechanism. *Nat. Med.* **15**, 545–552. https://doi.org/10.1038/nm.1960 (2009).
57. Wiig, H. et al. Immune cells control skin lymphatic electrolyte homeostasis and blood pressure. *J. Clin. Invest.* **123**, 2803–2815. https://doi.org/10.1172/JCI60113 (2013).
58. Goldman, J. et al. Regulation of lymphatic capillary regeneration by interstitial flow in skin. *Am. J. Physiol. Heart Circ. Physiol.* **292**, H2176-2183. https://doi.org/10.1152/ajpheart.01011.2006 (2007).
59. Chang, T. C., Uen, Y. H., Chou, C. H., Sheu, J. R. & Chou, D. S. The role of cyclooxygenase-derived oxidative stress in surgically induced lymphedema in a mouse tail model. *Pharm. Biol.* **51**, 573–580. https://doi.org/10.3109/13880209.2012.749923 (2013).
60. Mendez, U., Stroup, E. M., Lynch, L. L., Waller, A. B. & Goldman, J. A chronic and latent lymphatic insufficiency follows recovery from acute lymphedema in the rat foreleg. *Am. J. Physiol. Heart Circ. Physiol.* **303**, H1107-1113. https://doi.org/10.1152/ajpheart.00522.2012 (2012).
61. Morfoisse, F. et al. Lymphatic vasculature requires estrogen receptor-alpha signaling to protect from lymphedema. *Arterioscler. Thrombosis Vasc. Biol.* **38**, 1346–1357. https://doi.org/10.1161/ATVBAHA.118.310997 (2018).
62. Wang, K., Pan, Y., Tong, S., Liang, H. & Qiu, P. Deep-skin multiphoton microscopy of lymphatic vessels excited at the 1700-nm window in vivo. *Biomed. Opt. Express* **12**, 6474–6484. https://doi.org/10.1364/BOE.437482 (2021).
63. Shin, M. et al. Vegfc acts through ERK to induce sprouting and differentiation of trunk lymphatic progenitors. *Development* **143**, 3785–3795. https://doi.org/10.1242/dev.137901 (2016).

64. Okuda, K. S. et al. A zebrafish model of inflammatory lymphangiogenesis. *Biol. Open* **4**, 1270–1280. https://doi.org/10.1242/bio.013540 (2015).
65. Sanz, E. et al. Cell-type-specific isolation of ribosome-associated mRNA from complex tissues. *Proc. Natl. Acad. Sci. USA* **106**, 13939–13944. https://doi.org/10.1073/pnas.0907143106 (2009).
66. Miller, M. et al. Profiling the endothelial translatome in vivo using 'AngioTag' zebrafish. *bioRxiv*, https://doi.org/10.1101/815696 (2019).
67. Rossner, M. J. et al. Global transcriptome analysis of genetically identified neurons in the adult cortex. *J. Neurosci. Off. J. Soc. Neurosci.* **26**, 9956–9966. https://doi.org/10.1523/JNEUROSCI.0468-06.2006 (2006).
68. Llufrio, E. M., Wang, L., Naser, F. J. & Patti, G. J. Sorting cells alters their redox state and cellular metabolome. *Redox Biol.* **16**, 381–387. https://doi.org/10.1016/j.redox.2018.03.004 (2018).
69. Binek, A. et al. Flow cytometry has a significant impact on the cellular metabolome. *J. Proteome Res.* **18**, 169–181. https://doi.org/10.1021/acs.jproteome.8b00472 (2019).
70. Grimm, L. et al. Single-cell analysis of lymphatic endothelial cell fate specification and differentiation during zebrafish development. *EMBO J.* **42**, e112590. https://doi.org/10.15252/embj.2022112590 (2023).
71. Panara, V. et al. Multiple cis-regulatory elements control prox1a expression in distinct lymphatic vascular beds. *Development* **151**, https://doi.org/10.1242/dev.202525 (2024).
72. du Sert, N. P. et al. Reporting animal research: Explanation and elaboration for the ARRIVE guidelines 20. *PLoS Biol.* **18**, e3000411. https://doi.org/10.1371/journal.pbio.3000411 (2020).
73. Hall, C., Flores, M. V., Storm, T., Crosier, K. & Crosier, P. The zebrafish lysozyme C promoter drives myeloid-specific expression in transgenic fish. *BMC Dev. Biol.* **7**, 42. https://doi.org/10.1186/1471-213X-7-42 (2007).
74. Ellett, F., Pase, L., Hayman, J. W., Andrianopoulos, A. & Lieschke, G. J. mpeg1 promoter transgenes direct macrophage-lineage expression in zebrafish. *Blood* **117**, e49-56. https://doi.org/10.1182/blood-2010-10-314120 (2011).
75. Kwan, K. M. et al. The Tol2kit: A multisite gateway-based construction kit for Tol2 transposon transgenesis constructs. *Dev. Dyn. Offic. Publ. Am. Associat. Anat.* **236**, 3088–3099. https://doi.org/10.1002/dvdy.21343 (2007).

Acknowledgements

We are grateful to the UIC Biological Resource Laboratory for their assistance in zebrafish facility care. We also thank Ms. Michelle Dharma at UIC for her support in some of the experiments and her excellent care of the zebrafish used in this study. This research was supported by the American Heart Association (grant number 24PRE1199881) to O.O. and by the UIC College of Medicine start-up fund to H.M.J.

Author contributions

OO, HR, and HMJ performed the experiments and analyzed data. OO, XW, ABM, and HMJ contributed to the conceptualization and experimental design. OO and HMJ contributed to writing, reviewing, and editing the manuscript. HMJ conceived the study and supervised the work. All authors have read and agreed to the published version of the manuscript.

Declarations

Competing interests

The authors declare no competing interests.

Additional information

Supplementary Information The online version contains supplementary material available at https://doi.org/10.1038/s41598-025-92970-1.

Correspondence and requests for materials should be addressed to H.M.J.

Reprints and permissions information is available at www.nature.com/reprints.

Publisher's note Springer Nature remains neutral with regard to jurisdictional claims in published maps and institutional affiliations.